# Molecular Dynamics Simulations and Integral Equation Theory of Alkane Chains: Comparison of Explicit and United Atom Models

**Mesfin Tsige, John G. Curro,* and Gary S. Grest**

*Sandia National Laboratories, Albuquerque, New Mexico 87185*

**John D. McCoy**

*New Mexico Institute of Mining & Technology, Socorro, New Mexico 87801*

*Received August 2, 2002*

ABSTRACT: Molecular dynamics (MD) simulations and self-consistent polymer reference interaction site model (PRISM) calculations were performed on $C_{20}H_{42}$ and $C_{48}H_{98}$ liquids using an explicit atom (EA) model. Good agreement between theory and simulation was found for the intermolecular pair correlation functions $g_{HH}(r)$and $g_{CH}(r)$, but the PRISM theory tended to underestimate $g_{CC}(r)$. Good agreement was likewise found between theory and simulation with neutron diffraction measurements of $g_{HH}(r)$. MD and PRISM theory calculations were also performed on a united atom (UA) potential obtained from the EA potential by the UA/EA mapping procedure of McCoy and Curro [*Macromolecules* **1998**, *31*, 9362]. Excellent agreement between the liquid structure and chain dimensions from the UA and EA models was found. However, the full UA potential obtained from the UA/EA mapping exhibited attractions that were somewhat too strong as evidenced by a negative pressure and high compressibility. An empirical modification of the attractive tail of this UA potential leads to a modified UA potential that reproduces the EA pressure.

## 1. Introduction

As the simplest long chain polymer, the structure and dynamics of polyethylene (PE) melts have been extensively studied. The liquid-state structure factor obtained by wide-angle X-ray scattering[1−3] gives local information on how the polymer packs and serves as a valuable test for atomistic models, which have been studied by numerical simulation[4−13] and liquid state theory.[1,2,13] In developing atomistic models for both linear and branched alkanes, two approaches have been taken. The first is to treat all atoms explicitly as interaction sites, while in the second each carbon and its bonded hydrogen atoms are treated as a single united atom (UA). While explicit atom (EA) models are clearly more realistic, they require significantly greater computational effort to simulate due to both the larger number of interaction sites and the fact that the hydrogen atoms are light, resulting in a much smaller time step than for the UA models. For properties such as the vibrational spectrum, heat capacities, and elastic constants of crystalline polyethylene EA models are essential, while for studies of the static and dynamic structure of polyethylene, the UA models have been invaluable since one can study larger systems for longer times. For both cases the interaction between the explicit or united atoms consists of bonded and nonbonded pair interactions, usually Lennard-Jones or exp-6, along with bond bending and torsional interactions.

Since their first introduction, there have been numerous sets of classical interaction potentials for PE. Parameters for the EA potentials[7,14] have been estimated from ab initio calculations or obtained from experimental data (predominately crystal structure and properties), while UA parameters have for the most part been obtained empirically by fitting experimental data, such as the liquid/vapor coexistence curve[15,16] or the diffusion and structure of the short alkane melts.[17−19] However, there has been little effort in determining the interaction parameters for a UA potential from a corresponding EA potential for a given polymer. McCoy and Curro[20] have proposed such a procedure for carrying out a mapping of EA potentials onto UA potentials. One of the purposes of this investigation is to check the accuracy of this mapping by comparing the intermolecular pair correlation functions and equation of state obtained using the EA of Sorensen et al.[9] and the corresponding UA potential for polyethylene. Both MD simulations and PRISM theory are used for computing the melt structure.

Londono et al.[21] employed a method for uniquely extracting the intermolecular H/H pair correlation function $g_{HH}(r)$ from neutron diffraction experiments on mixtures of hydrogenated and deuterated alkanes. The only assumption required is that the structure and packing of the macromolecules is not affected by deuteration. Good agreement between the experimentally determined $g_{HH}(r)$ and MD simulations were observed for short chain alkanes[21] and polyethylene.[22] Here we will make similar comparisons of the experimental neutron diffraction data with intermolecular H/H pair correlation functions obtained from both MD simulations and polymer reference interaction site model (PRISM) theory.

The purpose of this paper is twofold. The first is to test the PRISM theory for an explicit atom model of polyethylene by comparing it directly to MD simulations for the same potential and to neutron diffraction experiments. The second is to test the recently proposed mapping procedure for obtaining a UA model from an EA model. In the next section, we will briefly describe the EA/UA mapping procedure as well as the MD and PRISM computational methods. The MD results for the intermolecular packing will then be compared with PRISM theory and experimental scattering data. A particular focus will be on the ability of the UA model, arising from the EA/UA mapping, to reproduce the melt

10.1021/ma0212543 CCC: $25.00 
Published on Web 02/27/2003

**Table 1. Nonbonded Potential Parameters**

| pair | $\epsilon$(kcal/mol) | $R_0$ (Å) | $\zeta$ | $\eta$ |
|---|---|---|---|---|
| Explicit Atom Model[7] | | | | |
| CC | 0.094813 | 3.8719 | 11.964 | 1 |
| CH | 0.052021 | 3.2739 | 11.180 | 1 |
| HH | 0.009777 | 3.3706 | 12.606 | 1 |
| United Atom Model from EA/UA Mapping[20] | | | | |
| $CH_2$ | 0.1817 | 4.32 | 7.2958 | 2.959 |
| $CH_2$ | 0.1817 | 4.32 | 16.072 | 1 |

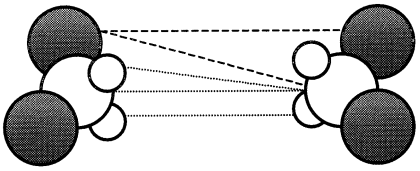

**Figure 1.** Schematic diagram of the chain fragments used to compute the UA potential for a $CH_2$ group in eq 3. The shaded circles represent UA sites, the large open circles represent carbon atoms, and the small open circles represent H atoms. The dotted lines depict EA potentials between atom pairs; the dashed lines depict UA potentials between $CH_2$ sites.

structure, pressure, and chain dimensions based on an explicit model of polyethylene.

## 2. Explicit and United Atom Models

In this work we use the model of Sorensen et al.[7] for the bond stretching, bond bending, and torsional potentials. The EA nonbonded potentials $V(r)$ were taken to have an exp-6 form

$$V(r) = V(r^*), \quad r \le r^*$$
$$= \epsilon\left\{\left(\frac{6}{\zeta-6}\right)\exp[\zeta(1-(r/R_0))] - \left(\frac{\zeta}{\zeta-6}\right)\left(\frac{R_0}{r}\right)^6\right\}, \quad r \ge r^* \quad (1)$$

The exp-6 potential is nonmonotonic in the repulsive regime and has a maximum at a separation $r^*$. In the MD simulations, separations $r < r^*$ are never accessed, and this cutoff is not relevant since $V(r^*)/k_BT$ is greater than 40 for the PE models studied here. However, in our PRISM calculations, single-chain Monte Carlo simulations using the pivot algorithm are employed, and it is important to modify the potential at short distances so that no two atoms overlap. The nonbonded potential parameters[7] are given in Table 1. Some of our MD and PRISM calculations were done on a repulsive EA potential obtained by shifting and clipping the potential in eq 1 to obtain an effective repulsive potential $V_R(r)$ following the method of Weeks, Chandler, and Andersen[23]

$$V_R(r) = V(r^*) + \epsilon, \quad r \le r^*$$
$$= V(r) + \epsilon, \quad r^* \le r \le R_0$$
$$= 0, \quad r \ge R_0 \quad (2)$$

McCoy and Curro[20] suggested an approximate mapping scheme whereby united atom potentials of a polymer can be constructed from knowledge of the explicit atom potentials. The method is based on a Monte Carlo simulation of two chain fragments held a fixed distance apart as depicted in Figure 1. $V(r)$ for a $CH_2$ site is obtained from the following averages

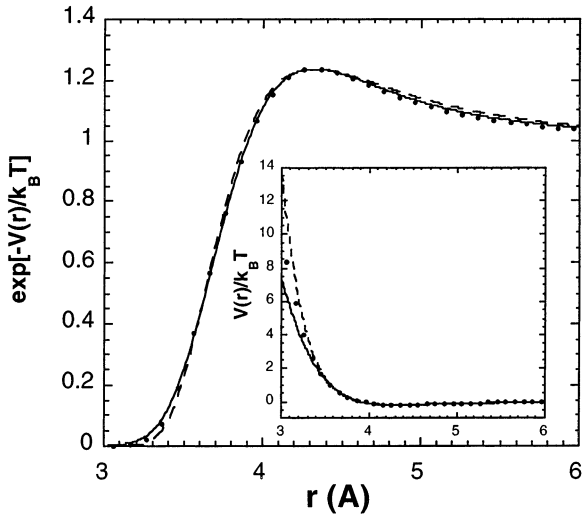


**Figure 2.** UA potential arising from the mapping procedure in eq 3. The points are the numerical data obtained from the Monte Carlo averaging. The solid curves are stretched exp-6 approximations, eq 4, to the numerical data with parameters given in Table 1. The dashed curves correspond to an exp-6 approximation to the numerical UA potential ($\eta = 1$) using parameters given in Table 1.

$$e^{-\beta V(r)} = \frac{\langle e^{-\beta U(r)}\rangle}{\langle e^{-\beta U(r)}\rangle_0} \quad (3)$$

where $\langle ...\rangle$ denotes the Monte Carlo average over all angular orientations of both fragments subject to the constraints that the carbon atoms are held a distance $r$ apart. $U(r)$ is the total potential energy of the fragment pair. The fragment was defined as an explicit atom $CH_2$ group attached to two UA sites. Thus, the potential energy is given by the pairwise sum of HH, CC, and CH EA interactions plus UA interactions between united atom pairs of sites illustrated by the dashed and dotted lines in Figure 1. The average with the subscript zero refers to the Monte Carlo average with the EA interactions turned off. Since the UA potentials appear on both sides of eq 3, the calculation must be performed self-consistently. One of the consequences of this mapping scheme is that, because of the averaging process in eq 3, the resulting UA potential is temperature-dependent.[20]

The EA/UA mapping was carried out for the explicit atom potential parameters in Table 1 at a temperature $T = 430$ K. The united atom potential for a $CH_2$ site that arises from this procedure is shown in Figure 2. For computational convenience, the numerical UA potentials that result from eq 3 can be fit to an analytical form that is a stretched exponential version of the exp-6 potential

$$V(r) = V(r^*), \quad r \le r^*$$
$$= \epsilon\left\{\left(\frac{6}{\eta\zeta-6}\right)\exp[\zeta(1-(r/R_0)^\eta)] - \left(\frac{\eta\zeta}{\eta\zeta-6}\right)\left(\frac{R_0}{r}\right)^6\right\} \quad (4)$$

The four parameters in this equation that fit the UA potential in Figure 2 are given in Table 1. A less accurate fit is achieved with the parameters in Table 1 by forcing eq 4 to the exp-6 form by constraining $\eta = 1$. The bond, angle, and dihedral potentials for the UA

model were standard potentials used in previous UA investigations.[15,25]

### 3. Computational Methods

Molecular dynamics is a very useful method to study the statistical mechanics of polymer systems since, in principle, formally exact results are obtainable. Starting configurations for the EA simulations of alkane chains of $C_{48}H_{98}$ and $C_{20}H_{42}$ were generated using the commercial Cerius$^2$ software package.[24] Sixty-five chains of $C_{48}H_{98}$ and 100 chains of $C_{20}H_{42}$ were grown in an amorphous structure in a cubic box with periodic boundary conditions. Starting configurations for the $N = 48$ UA model simulations with 400 chains were generated with a Monte Carlo technique using a standard pivot algorithm. The temperature and density for the simulations were $T = 323$ K and $\rho = 0.7888$ g/cm$^3$ for $C_{20}H_{42}$ and $T = 430$ K and $\rho = 0.7796$ g/cm$^3$ for $C_{48}H_{98}$.

The MD simulation consisted of two steps. First, to avoid overlaps between atoms that may have originated from the configuration generating algorithms, the atoms were initially "pushed off" by a soft, nonbonded potential until the actual potential could be switched on. After this initial push-off phase, the full simulation is then continued using the Nose−Hoover thermostat to simulate a canonical ensemble. The simulations were run using the LAMMPS code with a multiple time step second-order symplectic integrator (RESPA). An integration time step of 1 fs was used for the bond, 2 fs for the angle and torsion forces, and 4 fs for the nonbonded van der Waals forces. The nonbonded exp-6 potential is truncated and shifted at a cutoff of 6 Å. For the case of the EA model, the MD simulations were first equilibrated for approximately 1 ns, and then the atom positions were recorded every picosecond for at least another 1 ns for further analysis. For the UA model simulations, the positions of the $CH_2$ sites were saved every 20 ps.

Because of finite computer resources, the MD simulations are limited in practice to relatively small systems and short times. Integral equation methods such as PRISM theory can be also applied to the study of polymer melt structure. PRISM theory has the advantage of being much less demanding of computer resources, but the results are approximate because of the necessary closure approximation that is made. Nevertheless, good qualitative agreement has been found between PRISM theory predictions and the results from MD simulations[13,25,26] and wide-angle X-ray scattering experiments[1,2,26] for various polyolefin melts.

PRISM theory[27−29] is an extension to polymers of the reference interaction site model or RISM theory of Chandler and Andersen.[30,31] PRISM theory has been extensively discussed elsewhere,[29] and here it will only be outlined briefly. The starting point of the theory is the generalized Ornstein−Zernike equation,[29−31] which relates the intermolecular pair correlation functions $g_{\alpha\gamma}(r) = h_{\alpha\gamma}(r) + 1$ to the intramolecular structure factor $\hat{\Omega}_{\alpha\gamma}(k)$. In Fourier transform space the generalized Ornstein−Zernike equation can be conveniently written in matrix notation as

$$\hat{\mathbf{H}}(k) = \hat{\mathbf{\Omega}}(k) \cdot \hat{\mathbf{C}}(k) \cdot [\hat{\mathbf{\Omega}}(k) + \hat{\mathbf{H}}(k)] \tag{5}$$

where the caret denotes Fourier transformation with wave vector $k$. $H_{\alpha\gamma}(r) = \rho_\alpha \rho_\gamma h_{\alpha\gamma}(r)$, where $\rho_\alpha$ is the density of atoms or sites of type α. $\mathbf{C}(r)$ is the direct correlation function[32] matrix defined through eq 5. The average intramolecular structure of a chain of $N$ sites is specified through the single chain structure factor defined as

$$\hat{\Omega}_{\alpha\gamma}(k) = \frac{\rho_\alpha}{N_\alpha} \sum_{i \in \alpha}^{N_\alpha} \sum_{j \in \gamma}^{N_\gamma} \left\langle \frac{\sin(kr_{ij})}{kr_{ij}} \right\rangle \tag{6}$$

where the summations over $i$ and $j$ range over $N_\alpha$ sites of types α and $N_\gamma$ sites of type $\gamma$ on a given chain. By analogy with the Percus−Yevick theory[32] of atomic liquids, in PRISM theory we approximate the direct correlation function according to the closure relation[29]

$$C_{\alpha\gamma}(r) \cong \{1 - \exp[\beta V_{\alpha\gamma}(r)]\} g_{\alpha\gamma}(r) \tag{7}$$

In small molecule and atomic liquids, it is well established[32] that at liquidlike densities the liquid packing is dominated by the repulsive part of the potential. Attractions are very important in determining thermodynamic properties but, provided they are weak, do not significantly affect the intermolecular pair correlations. Comparisons with simulations suggest that weak attractions also do not appreciably affect the structure of polymer melts.[13,25] Since PRISM theory has been found[29] to be most accurate for repulsive potentials, we used the repulsive, exp-6 potential in eq 2 in all of the PRISM computations presented here.

For a given intramolecular structure function $\hat{\Omega}_{\alpha\gamma}(k)$, eqs 5 and 7 can be solved numerically to compute the intermolecular pair correlation functions of polyethylene in the melt state. In the melt state it is known that polymer chains adopt dimensions close to ideal chains where the long-range excluded-volume interactions are screened. In this case $\hat{\Omega}_{\alpha\gamma}(k)$ can be estimated from a model with no long-range repulsive interactions.[29] More accurate calculations, however, require that the intramolecular structure and intermolecular packing correlations be calculated self-consistently.[25,26,29] This can be achieved by performing a single chain Monte Carlo simulation for the polymer with all the intramolecular repulsive interactions turned on. The remaining chains in the melt are mimicked through pairwise additive, intramolecular "solvation potential" $W_{\alpha\gamma}(r)$ acting between all pairs of intramolecular sites. In Fourier space, an approximate form of this solvation potential is given by[33,34]

$$\beta \hat{\mathbf{W}}(k) = -\hat{\mathbf{C}}(k) \cdot \hat{\mathbf{S}}(k) \cdot \hat{\mathbf{C}}(k) \tag{8}$$

where $\hat{S}_{\alpha\gamma}(k)$ is the structure factor matrix defined according to

$$\hat{S}_{\alpha\gamma}(k) = \rho_\alpha \hat{\Omega}_{\alpha\gamma}(k) + \rho_\alpha \rho_\gamma \hat{h}_{\alpha\gamma}(k) \tag{9}$$

At short distances the solvation potential is generally attractive and serves to counterbalance the repulsive, intramolecular, excluded-volume interactions. The essence of the Flory ideality hypothesis is that the excluded-volume and solvation forces effectively cancel each other.

From eq 8 it can be seen that the solvation potential involves both $C_{\alpha\gamma}(r)$ and $g_{\alpha\gamma}(r)$ determined from eqs 5 and 7. However, these equations also require a knowledge of the intramolecular structure and hence the

solvation potential. A self-consistent solution can be obtained by first guessing $W_{\alpha\gamma}(r)$, calculating $\hat{\Omega}(k)$ from a single chain Monte Carlo simulation, and then solving the PRISM theory for $C_{\alpha\gamma}(r)$ and $g_{\alpha\gamma}(r)$, leading to a new estimate of the solvation potential. This process is repeated until $W_{\alpha\gamma}(r)$ does not change from one iteration to the next within some tolerance. In practice, one can avoid performing a new Monte Carlo simulation for each iteration by employing a reweighting technique.[25] The single chain Monte Carlo simulations in our self-consistent PRISM calculations used a standard pivot algorithm.[25]

From the above discussion, it can be seen that PRISM theory effectively maps the many-chain MD simulation to a much simpler single-chain Monte Carlo simulation. The price one pays for this simplification, however, is that the calculation is no longer exact because of the approximations made in the closure relation and in the solvation potential.

Equations 5−9 for the PRISM theory have been written in matrix notation and can be applied to the explicit atom model to predict the three intermolecular radial distribution functions involving C and H atoms: $g_{CC}(r)$, $g_{CH}(r)$, $g_{HH}(r)$. These equations can also be applied to the united atom model to estimate the intermolecular correlation function $g(r)$ between $CH_2$ sites on different polyethylene chains in the melt.

## 4. Results and Discussion

In previous work,[13] comparisons were made between MD simulations and PRISM theory for a united atom potential, where it was found that PRISM theory underestimates the melt structure and overestimates the compressibility. Here we made a similar comparison using an explicit atom potential. MD simulations were performed using the exp-6 potential with the parameters given in Table 1. Self-consistent PRISM calculations were carried out using the same parameters but with the shifted repulsive version of the exp-6 potential prescribed by eq 2.

Results for the $C_{20}H_{42}$ alkane liquid are shown in Figure 3 while the results for the $C_{48}H_{98}$ alkane liquid are shown in Figure 4. It can be seen from both of these figures that good agreement exists between theory and simulation for $g_{HH}(r)$ and $g_{CH}(r)$. However, in the case of $g_{CC}(r)$ between intermolecular carbon atoms, the agreement between PRISM and MD is less satisfactory. In particular, we see that PRISM predicts significantly less structure in the CC correlation function than observed in the simulation as was found earlier[13] in polyethylene with the UA model. The fact that PRISM is not as accurate for $g_{CC}(r)$ is also consistent with previous work[25] on polypropylene and polyisobutylene. In this previous study it was found that PRISM theory is most accurate in describing correlations between exposed $CH_3$ sites attached to the chain backbone and least reliable in predicting correlations between shielded backbone carbons.

The pressures deduced from the EA model for both systems are shown in Table 2. A small tail correction to the pressure was applied beyond a cutoff distance of 12 Å. Note that at the densities studied the pressures resulting from the explicit atom model are somewhat larger than atmospheric pressure. These results suggest that this particular EA model is not well calibrated for thermodynamic properties.

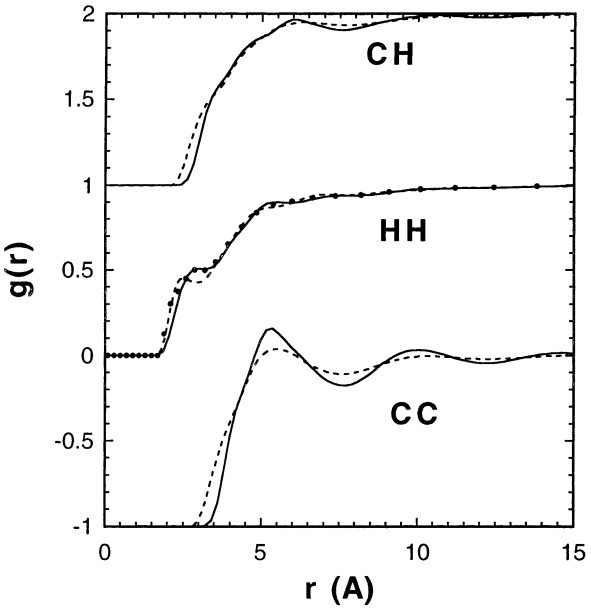


**Figure 3.** Three intermolecular radial distribution functions for $C_{20}H_{42}$ obtained from MD simulations (solid curves) and PRISM theory (dashed curves) at $T = 323$ K and density 0.7888 g/cm$^3$. The experimental $g_{HH}(r)$ obtained from neutron diffraction[21] is given by the points.

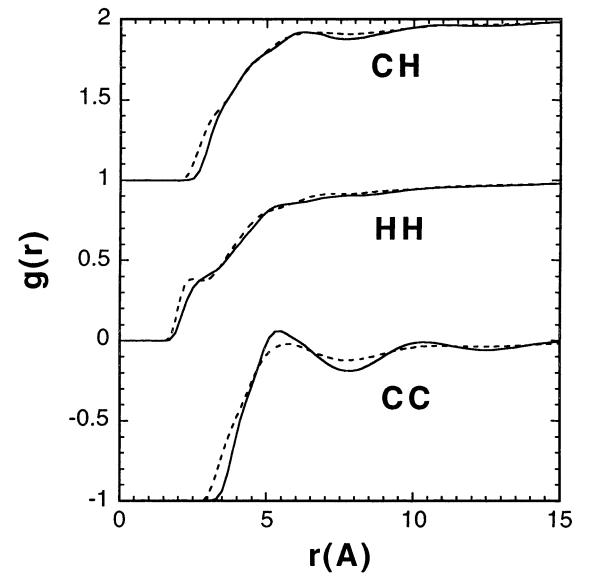


**Figure 4.** Three intermolecular radial distribution functions for $C_{48}H_{98}$ obtained from MD simulations (solid curves) and PRISM theory (dashed curves) at $T = 430$ K and density 0.7796 g/cm$^3$.

**Table 2. Pressure (atm)**

| model | $C_{20}H_{22}$ | $C_{48}H_{98}$ |
|---|---|---|
| EA | 183 ± 11 | 302 ± 10 |
| UA | | −701 ± 6 |
| UA repulsion | | 4381 ± 6 |
| UA ($\alpha = 0.25$) | | 298 ± 6 |

Londono and co-workers[21] directly measured the radial distribution function between hydrogen atoms from deuterium substitution experiments on $C_{20}H_{42}$ with neutron diffraction. Their results are also plotted in Figure 3 where it can be seen that both the simulation and theory are in accordance with experiment. Similar agreement between MD and experiment was reported previously[21] on $C_{13}H_{28}$. It can be seen that both MD and PRISM reproduce the shoulder in $g_{HH}(r)$ in the

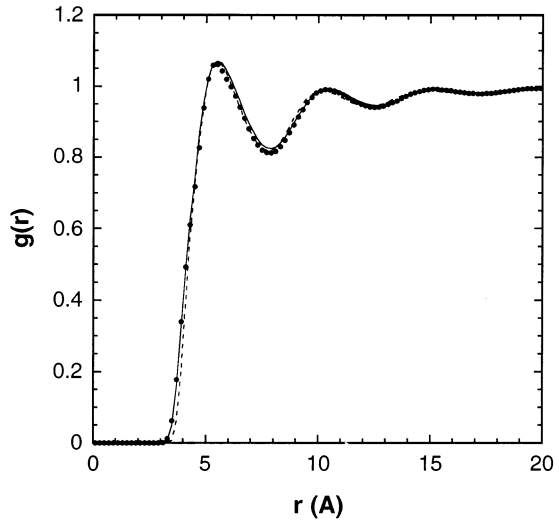


**Figure 5.** Radial distribution function $g_{CC}(r)$ for $C_{48}H_{98}$ obtained from MD simulations at $T = 430$ K and density 0.7796 g/cm$^3$. The points are for the EA model with attractions on. The dashed (solid) line is for the UA model with attractions on (off). The same solid curve, within the error of the simulation, was obtained from the modified form of the UA potential with attractions for $\alpha = 0.25$.

2.0−3.5 Å range. To investigate the origin of this structural feature, we computed the equivalent hard-core distance between H atoms from the formula[32]

$$d = \int_0^\infty [1 - e^{-\beta V(r)}]\, dr \qquad (10)$$

From the shifted exp-6 potential and the HH potential parameters from Table 1, the hard-core distance between hydrogen atoms is approximately 2.2 Å. The shoulder in $g_{HH}(r)$ is probably due to this preferred interatomic distance.

Given an explicit atom potential, can we construct a united atom potential that leads to a liquid with similar structure and thermodynamics? To address this question, we explored the ability of our UA/EA mapping procedure to produce an accurate potential. Accordingly, MD simulations were performed using the numerical UA potential depicted in Figure 2. For computational convenience one could employ the stretched exp-6 approximation with good accuracy using the parameters given in Table 1. It can be seen from Figure 2 that this analytical form is an excellent approximation to the numerical potential. The full UA potential, and the effective repulsive potential determined according to eq 2, were studied. In Figure 5 we plotted the intermolecular radial distribution function of $CH_2$ sites obtained from both the full and repulsive UA potentials along with $g_{CC}(r)$ obtained from the EA model. It can be seen that the intermolecular packing resulting from the UA model is in quantitative agreement with the EA model. As expected from conventional liquid state theory, it can be seen that the attractions do not significantly affect the intermolecular packing. Thus, we see that our UA/EA mapping procedure is very accurate for predicting the liquid structure.

In Table 2 we observe that the pressure resulting from the full UA model is negative in contrast to the EA pressure, suggesting that the UA attractions are too large. This is confirmed by comparing the structure factors resulting from the full and repulsive UA potentials as seen in Figure 6. Note that there are differences

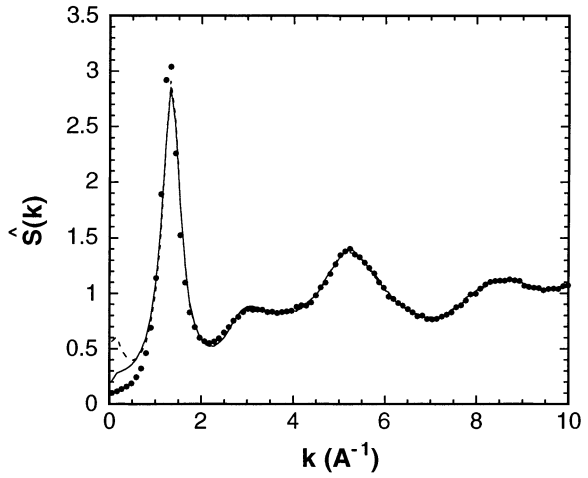


**Figure 6.** Structure factor $\hat{S}(k)$ for $C_{48}H_{98}$ for the UA model obtained from simulations at $T = 430$ K and density 0.7796 g/cm$^3$. The dashed curve is for the original potential including attractions ($\alpha = 0$). The points are for the purely repulsive form of the potential. The solid curve is for the case $\alpha = 0.25$.

in $\hat{S}(k)$ at low wave vectors. In particular, the zero wave vector limit of the structure factor with attractive interactions turned on is larger than in the purely repulsive case. Since $\hat{S}(0) = \rho k_B T \kappa_T$, it is clear that the attractions in the UA are somewhat too large, resulting in a compressibility that is larger than in the EA model. Although the UA/EA mapping is accurate for the liquid structure, it fails to reproduce the EA equation of state.

To correct this problem, we empirically adjusted the range of the attractive part of the UA potential according to

$$V_m(r) = V(r), \quad r \le R_0$$
$$= V(r) \exp[-\alpha(r - R_0)^2], \quad r \ge R_0 \qquad (11)$$

while leaving the repulsive part of the potential unchanged. The parameter $\alpha$ can be adjusted to obtain the desired pressure between that of the unmodified (−701 atm) and the purely repulsive potential (4381 atm) as seen in Figure 7. To approximately match the EA pressure, a value of $\alpha = 0.25$ was used. The full and modified UA potentials are shown in Figure 7 in the attractive regime. With this modified form of the attractive interaction, we find, as expected, that the same liquid structure is obtained as before as seen in Figure 5. However, now there is good agreement between compressibility of the UA and EA models as seen in Figure 6 at low vectors. Another measure of the adequacy of the UA potential is its ability to reproduce the single chain dimensions of the EA model. Table 3 gives the results of the mean-square end-to-end distances $\langle R^2 \rangle$ for the two models. It can be seen that the UA and EA models are in close agreement (∼3%).

As a final test of the UA/EA mapping, we compared the structural correlations predicted from PRISM theory with both the EA and UA models. In both models we used the repulsive version of the potentials $V_R(r)$ following eq 2. In the case of the UA potential, we employed the exp-6 approximation rather than the more accurate stretched exp-6 representation of the numerical data. The exp-6 UA parameters are given in Table 1. This form of the potential is seen to be a good approximation to the actual numerical potential in Figure 2. The radial distribution functions from PRISM calcu-

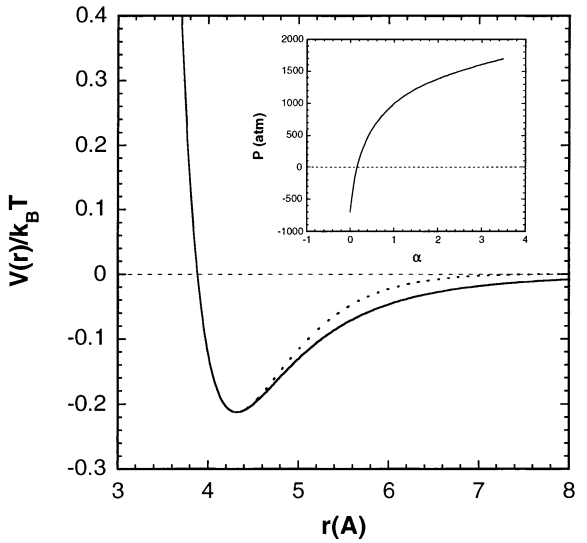


**Figure 7.** Original UA potential (solid line) from the mapping procedure in eq 3 and the modified UA potential (dashed curve) obtained by adjusting the range of the attractive tail according to eq 11 to obtain the same pressure as for the EA model.

**Table 3. Mean-Square End-to-End Distance for $C_{48}H_{98}$**

| model | MD | PRISM |
|---|---|---|
| EA | 906 ± 5 | 915.5 ± 6 |
| UA | 875 ± 3 | |
| UA repulsion | 882 ± 4 | 908.5 ± 9 |
| UA (α = 0.25) | 880 ± 5 | |

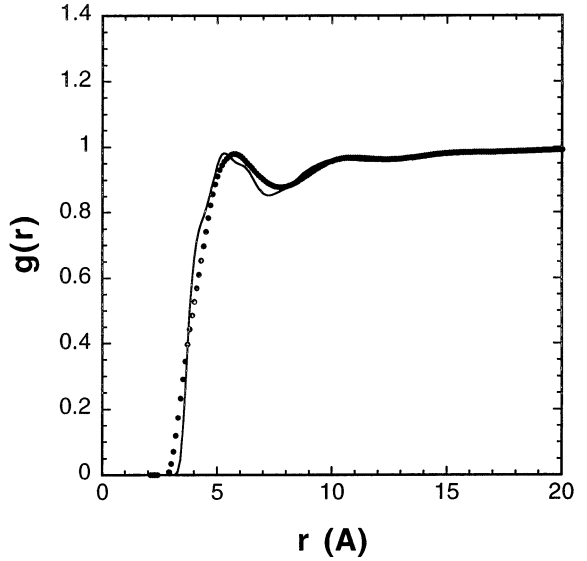


**Figure 8.** Radial distribution function $g_{CC}(r)$ for $C_{48}H_{98}$ obtained from PRISM theory at $T = 430$ K and density 0.7796 g/cm$^3$. The points (solid curve) are for the EA (UA) model for the purely repulsive form of the potential.

lations on the two models are plotted in Figure 8 where we observe that the agreement between the PRISM predictions of the two models is quite good. Good agreement of the UA and EA models is likewise found for the structure factor as seen in Figure 9. It should be emphasized that since only the repulsive parts of the two potentials were used, the problems related to the large UA attractions that we saw in the MD simulations do not arise in the PRISM calculations. In Table 3, we see that the chain dimensions calculated from self-consistent PRISM theory from the two models are in close agreement.

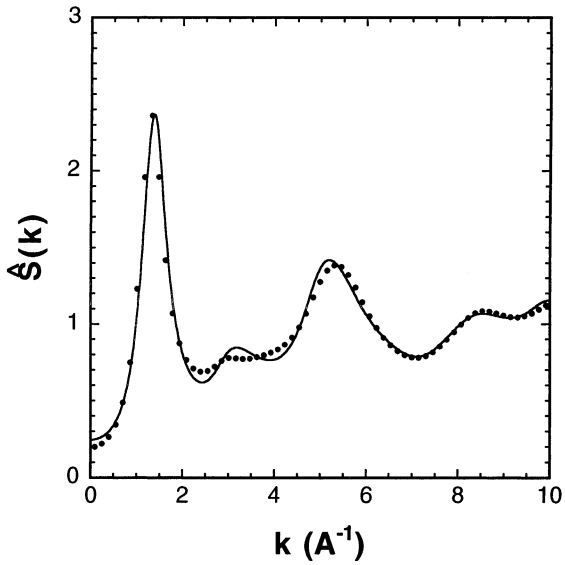


**Figure 9.** Structure factor $\hat{S}(k)$ for $C_{48}H_{98}$ obtained from PRISM theory at $T = 430$ K and density 0.7796 g/cm$^3$. The points (solid curve) are for the EA (UA) model for the purely repulsive form of the potential.

## 5. Conclusions

In this paper we investigated moderate length alkane chain molecules in the liquid state to address several issues related to the intermolecular packing. We found that PRISM theory accurately predicts the HH and CH intermolecular correlation functions. As found in previous studies, PRISM theory is less accurate in predicting correlations between backbone sites, in this case $g_{CC}(r)$, than correlation functions between pendant sites. Good agreement was found between both theory and simulation with $g_{HH}(r)$ obtained directly from neutron diffraction experiments on alkane liquids. We also compared predictions from explicit and united atom potentials.

On the basis of our MD simulations and PRISM calculations, it appears that the UA/EA mapping procedure of McCoy and Curro[20] leads to a UA model that is able to accurately reproduce the liquid packing and chain dimensions of the explicit atom model. However, the full UA potential (with attractions) has too strong an attractive tail, leading to a negative pressure and large compressibility. To achieve better agreement for the equation of state, it was necessary to slightly attenuate the effects of the UA attractions in an ad hoc fashion. The necessity for this modification is not surprising when one considers the simplicity of the mapping procedure. The Monte Carlo averaging of the chain fragments depicted in Figure 1 is clearly an oversimplification, since only the shielding effects of adjacent monomers on a $CH_2$ group are taken into account. This could be improved by considering longer chain fragments. Moreover, condensed phase effects are also ignored since only a pair of fragments is considered. Condensed phase effects could be incorporated into the mapping through a medium-induced solvation potential determined from a full MD simulation of PRISM theory.

**Acknowledgment.** The authors thank Mathias Pütz for performing some of the self-consistent PRISM calculations and Brian Annis for making his neutron diffraction data available to us. Sandia is a multiprogram laboratory operated by Sandia Corporation for the US Department of Energy under Contract DE-AC04-94AL85000.

## References and Notes


(1) Honnell, K. G.; McCoy, J. D.; Curro, J. G.; Schweizer, K. S.; Narten, A.; Habenschuss, A. *J. Chem. Phys.* **1991**, *94*, 4659.
(2) Narten, A.; Habenschuss, A.; Honnell, K. G.; McCoy, J. D.; Curro, J. G.; Schweizer, K. S. *J. Chem. Soc., Faraday Trans.* **1992**, *88*, 1791.
(3) Londono, J. D.; Habenschuss, A.; Curro, J. G.; Rajasekaran, J. J. *J. Polym. Sci., Part B* **1996**, *34*, 3055.
(4) Weber, T. A.; Helfand, E. *J. Chem. Phys.* **1979**, *71*, 4760.
(5) Vacatello, M.; Avitabile, G.; Corradini, P.; Tuzi, A. *J. Chem. Phys.* **1980**, *73*, 548.
(6) Rigby, D.; Roe, R.-J. *J. Chem. Phys.* **1987**, *87*, 7285.
(7) Sorensen, R. A.; Liau, W. B.; Kesner, L.; Boyd, R. H. *Macromolecules* **1988**, *21*, 200.
(8) Boyd, R. H. *Macromolecules* **1989**, *22*, 2477. Boyd, R. H.; Pant, P. V. K. *Macromolecules* **1991**, *24*, 4078. Jin, Y.; Pernice, M.; Boyd, R. H. *Comput. Theor. Polym. Sci.* **1996**, *6*, 9.
(9) Yoon, D. Y.; Smith, G. D.; Matsuda, T. *J. Chem. Phys.* **1993**, *98*, 10037.
(10) Smith, G. D.; Yoon, D. Y. *J. Chem. Phys.* **1994**, *100*, 649. Paul, W.; Smith, G. D.; Yoon, D. Y. *Macromolecules* **1997**, *30*, 7772.
(11) Dodd, L. R.; Theodorou, D. N. *Adv. Polym. Sci.* **1994**, *116*, 249. Uhlherr, A.; Mavrantzas, V. G.; Doxastakis, M.; Theodorou, D. N. *Macromolecules* **2001**, *34*, 8554. Marvantzas, V. G.; Boone, T. D.; Zervopoulou, E.; Theodorou, D. N. *Macromolecules* **1999**, *32*, 5072.
(12) Mondello, M.; Grest, G. S.; Webb, E. B.; III; Peczak, P. *J. Chem. Phys.* **1998**, *109*, 798.
(13) Curro, J. G.; Webb III, E. B.; Grest, G. S.; Weinhold, J. D.; Pütz, M. *Macromolecules* **1999**, *111*, 9073.
(14) A comparison of the performance of three explicit atom models for the density and heat of vaporization for short alkanes is given in: Kaminski, G.; Jorgensen, W. L. *J. Phys. Chem.* **1996**, *100*, 18010 and for the liquid vapor phase diagram in: Chen, B.; Martin, M. G.; Seipmann, J. I. *J. Phys. Chem. B* **1998**, *102*, 2578.
(15) Martin, M. G.; Siepmann, J. I. *J. Phys. Chem. B* **1998**, *102*, 2569.
(16) Nath, S. K.; Escobedo, F. A.; de Pablo, J. J. *J. Chem. Phys.* **1998**, *108*, 9905.
(17) Jorgensen, W. L.; Madura, J. D.; Swenson, C. J. *J. Am. Chem. Soc.* **1984**, *106*, 6638.
(18) Padilla, P.; Toxvaerd, S. *J. Chem. Phys.* **1991**, *94*, 5650; *J. Chem. Phys.* **1991**, *95*, 509.
(19) Paul, W.; Yoon, D. Y.; Smith, G. D. *J. Chem. Phys.* **1995**, *103*, 1702.
(20) McCoy, J. D.; Curro, J. G. *Macromolecules* **1998**, *31*, 9362.
(21) Londono, J. D.; Annis, B. K.; Turner, J. Z.; Soper, A. K. *J. Chem. Phys.* **1994**, *101*, 7868.
(22) Londono, J. D.; Annis, B. K.; Habenschuss, A.; Smith, G. D.; Borodin, O.; Tso, C.; Hsieh; Soper, A. K. *J. Chem. Phys.* **1999**, *110*, 8786.
(23) Weeks, J. D.; Chandler, D.; Andersen, H. C. *J. Chem. Phys.* **1971**, *54*, 5237.
(24) Cerius2 Simulation Tools User's Reference, Molecular Simulations Inc., Cambridge, MA, 1994.
(25) Pütz, M.; Curro, J. G.; Grest, G. S. *J. Chem. Phys.* **2001**, *114*, 2847.
(26) Weinhold, J. D.; Curro, J. G.; Habenschuss, A.; Londono, J. D. *Macromolecules* **1999**, *32*, 7276.
(27) Schweizer, K. S.; Curro, J. G. *Phys. Rev. Lett.* **1987**, *58*, 246.
(28) Curro, J. G.; Schweizer, K. S. *Macromolecules* **1987**, *20*, 1928.
(29) For reviews see: Schweizer, K. S.; Curro, J. G. *Adv. Polym. Sci.* **1994**, *116*, 321; *Adv. Chem. Phys.* **1997**, *98*, 1.
(30) Chandler, D.; Andersen, H. C. *J. Chem. Phys.* **1972**, *57*, 1930.
(31) Chandler, D. In *Studies in Statistical Mechanics VIII*; Montroll, E. W., Lebowitz, J. L., Eds.; North-Holland: Amsterdam, 1982; p 274.
(32) Hansen, J. P.; McDonald, I. R. *Theory of Simple Liquids*, 2nd ed.; Academic Press: London, 1986.
(33) Chandler, D.; Singh, Y.; Richardson, D. M. *J. Chem. Phys.* **1984**, *81*, 1975.
(34) Nichols, A. L.; Chandler, D.; Singh, Y.; Richardson, D. M. *J. Chem. Phys.* **1984**, *81*, 5109.


MA0212543